ISSN: 2692-5397
DOI: 10.33552/MCMS.2023.05.000613
Modern Concepts in Material Science
Iris Publishers

Research Article

A Review on the Properties and Electronic Applications of Glass Fibers: Effect of Radiation

Mohammad A Amin, Samiul A Khan, Farjana Islam and Ruhul A Khan*

Polymer Composite Laboratory, Institute of Radiation and Polymer Technology, Atomic Energy Research Establishment, Savar, Dhaka, Bangladesh.

***Corresponding author:** Ruhul A Khan, Polymer Composite Laboratory, Institute of Radiation and Polymer Technology, Atomic Energy Research Establishment, Savar, Dhaka, Bangladesh.

Received Date: October 09, 2023

Published Date: October 25, 2023

Abstract

This review article presents an overview of research dedicated to the examination of interfaces in polymers that are reinforced with glass fibers, electronic applications and effects of radiations. It delves into discussions concerning the chemical and mechanical properties, thermal performance, vibrational behavior, and water absorption of glass fibers. These aspects play a crucial role in linking the polymer matrix with the reinforcing element. Additionally, the article highlights how these interphases influence the overall mechanical properties of fiber-reinforced composites. Today, glass fibers have a wide range of applications in industries such as electronics, aviation, and automotive. They are prized for their impressive qualities, which include exceptional strength, flexibility, stiffness, and resistance to chemical corrosion. Glass fibers come in various forms, including rovings, chopped strands, yarns, fabrics, and mats. Each type of glass fiber has unique properties, making them suitable for specific uses in polymer composites. Researchers have extensively studied the mechanical, tribological, thermal, water absorption, and vibrational characteristics of polymer composites reinforced with different types of glass fibers.

Keywords: Mechanical properties; Molecular characterization; Tensile properties; Thermal behavior; Electronic Properties; Vibration behavior; Water absorption

Introduction

This review article works the polymers reinforced with glass fibers. It offers explanations about the chemical and mechanical attributes, Thermal behavior, vibrational behavior and water absorption of the glass fiber, which connect the polymer matrix to the reinforcing component. Furthermore, the article outlines the impacts of these interphases on the overall mechanical characteristics of composites strengthened by fibers [1].

In contemporary times, glass fibers find application across electronics, aviation, automobiles, and more. These fibers boast outstanding qualities such as remarkable strength, flexibility, stiffness, and resistance to chemical damage. They manifest in diverse forms, including rovings, chopped strands, yarns, fabrics, and mats. Each variant of glass fiber possesses distinct characteristics, catering to different applications within polymer composites. Researchers have documented the mechanical, tribological, thermal, water absorption, and vibrational attributes of a range of polymer composites strengthened with various types of glass fibers [2].

Glass fiber is a substance comprising numerous incredibly thin strands of glass. Over time, artisans have conducted trials with glass fibers; however, large-scale production of these fibers became achievable only after the development of more advanced machine tools. Composite materials offer a unique synergy of properties that are unattainable when using either the fibers or matrix material individually. For decades, fiber-reinforced composites have proven successful in a wide range of engineering applications. Among these composites, Glass Fiber-Reinforced Polymeric (GFRP) materials have been particularly prevalent. These GFRP composites typically utilize matrices composed of various organic resins, including polyester, thermostable, vinylester, phenolic, and epoxy resins. Polyester resins, for instance, can be classified as bisphenol, ortho, or isophthalic. The mechanical performance of a fiber-reinforced

composite hinges on several key factors. These include the strength and modulus of the fibers, the chemical stability of the matrix, the strength of the matrix material itself, and the quality of the interface bonding between the fibers and matrix, which is essential for effective stress transfer.

By carefully selecting the composition and orientation of the fibers, it becomes possible to achieve specific desired properties and functional characteristics in GFRP composites. In some cases, these composites can rival the properties of steel, boasting higher stiffness than aluminum, all while maintaining a significantly lower specific gravity, just a quarter of that of steel.

Moreover, GFRP composites can be tailored for enhanced performance through various types of glass fiber reinforcements, including long longitudinal fibers, woven mats, distinct chopped fibers, and chopped mats. Ultimately, the properties of these composites are heavily influenced by the specific fibers incorporated and their arrangement within the matrix during the composite fabrication process.

History of Glass Fiber

Glass fiber experimentation dates back to ancient times, but large-scale production commenced in 1893 when Edward Drummond Libbey showcased a fabric blend of silk and glass fiber, marking the inception of mass glass fiber manufacturing [3]. In 1938, Russell Games Slayter secured the first patent for glass wool production, yielding fibers with commendable electrical insulation properties, leading to their classification as 'electrical glass' or E-glass. Beginning in 1939, glass fibers found application as insulators in US navy warships. The progression continued through World War II, where glass fiber manufacturing played a pivotal role, especially in tandem with unsaturated polyester resin production, resulting in the creation of radar domes and aircraft structural components through hand layup techniques. A significant milestone emerged in 1953 when General Motors initiated large-scale production of Chevrolet Corvette sports car bodies using glass fiber and the sheet molding compound (SMC) technique. Technological advancements, growing consumer consciousness, and government regulations prompted substantial investments by glass fiber manufacturers to minimize waste. Notably, the reduction of furnace emissions, primarily dust, sulfur dioxide, and nitrogen oxides, emerged as a prominent challenge. The adoption of oxygen combustion proved advantageous in curbing nitrogen oxide emissions. To address environmental concerns, glass manufacturers adopted the production of fluorine- and boron-free glasses, aiming to mitigate fluorine pollution and reduce air pollutants during the manufacturing process. Constant industrial demands have been a catalyst for the creation of novel fibers featuring elevated mechanical strength and corrosion resistance. As a response, various types of glasses, such as S glass, ECR glass, and boron-free glass, have been developed [4].

Since the publication of the initial edition in 1972, the glass fiber sector has encountered the typical challenges faced by various industries, undergoing significant transformations as a consequence. The Yom Kippur War in 1973 marked the end of affordable energy, resulting in escalated energy expenses. These cost hikes subsequently triggered widespread increases in both material and labor costs, which began to show signs of subsiding during a period of sluggish industrial performance in 1981. Simultaneously, the escalating environmental impacts of expanding industrial operations necessitated the implementation of pollution controls. In the context of the glass fiber industry, the focus was on curtailing emissions from glass furnace chimneys and mitigating the pollution present in wastewater discharged from plants. Achieving these pollution reduction targets demanded substantial investments and, in some instances, alterations to technology. During this same timeframe, the largest player in the field, Owens-Corning Fiberglas, successfully defended itself against a takeover attempt facilitated by external actors utilizing what are colloquially referred to as 'junk bonds. In the current economic downturn (1992), glass fiber sales have remained stagnant since 1989, prompting the industry to pursue further streamlining measures. Disposal of outdated machinery and equipment has been carried out, and smaller manufacturers in developed countries have all but vanished [3].

Types of Glass fiber

Delicate threads of silica-based material, such as SiO2, or other designed glass compositions, are extruded into numerous fine fibers with small diameters. These fibers are well-suited for applications like textile production and are created as staple fibers, essentially naturally occurring groupings or bundles reminiscent of wool fibers [5, 6]. The glass fibers typically used in Fiber-Reinforced Composites (FRCs) are E-glass and S-glass fibers. E-glass fiber has a composition comprising approximately 54.5 wt% SiO2, 14.5 wt% Al2O3, 17 wt% CaO, 4.5 wt% MgO, 8.5 wt% B2O3, and 0.5 wt% Na2O. On the other hand, S-glass fiber consists of 64 wt% SiO2, 26 wt% Al2O3, and 10 wt% MgO [5, 7]. In Table (1), the types of glass fiber are listed.

Glass fibers that are readily accessible in the market are shaped into strands, chopped strands, woven rovings, or woven cloth (also known as veil). Within strands, these fibers can come together to create bundles comprising 200 or more parallel individual filaments. Chopped strands are what remain after continuous strands are cut into shorter lengths. Woven roving entails a textile where continuous rovings are woven along two perpendicular directions. Woven cloth and veil denote fabrics woven from twisted continuous strands [5].

Table 1: Types of Glass Fibers [5, 7].

Type	Manufacturing	Composition	Characteristics	Applications
A-Glass	Derived from recycled glass, often sourced from used bottles, and transformed into fiber.	Alkali-lime composition containing minimal or no boron oxide	Displays limited resistance against alkali	Suitable when there is no need for alkali resistance.
AR-Glass			Exhibits alkali resistance	Necessary in cases where alkali resistance is needed.
C-Glass (T-Glass)	Obtained by processing used glass staple fibers	Alkali-lime glass with elevated boron oxide content.	Shows resistance against chemical attacks & most acids that can dissolve E-glass.	Used when enhanced chemical resistance to acids is necessary, such as in the case of glass staple fibers.
D-Glass		Borosilicate	Prominent dielectric constant	Preferable when a significant dielectric constant is desired
E-Glass		Comprises alumino-borosilicate with less than 1 wt% alkali oxides	Not resistant to chloride ions; the surface of E-glass is soluble.	Initially designed for electrical applications, now primarily used in glass-reinforced plastics
E-CR Glass		Comprises alumino-lime silicate with less than 1 wt% alkali oxides	Ideal for situations demanding strong resistance to acids.	Essential when exceptional acid resistance is needed
R-Glass		Alumino silicate composition lacking MgO or CaO	Displays favorable mechanical properties	Suited for applications with elevated mechanical demands
S-Glass		S-glass, composed of alumino silicate without CaO but enriched with high MgO content	Boasts the highest tensile strength among all fiber types	Utilized in aircraft components and missile casings, particularly when a high tensile strength is required

Table 1.1: Abbreviations and Attribute [8, 9].

Abbreviations	Attribute
Electrical Glass (E-Glass)	Minimal electrical conductivity
Strength Glass (S-Glass)	Remarkable strength
Chemical Glass (C- Glass)	Elevated chemical resistance
Modulus Glass (M-Glass)	Remarkable stiffness
Alkali Glass (A Glass)	Remarkable alkali
Dielectric Glass (D Glass)	Minimal dielectric constant

Table 2: Different types of Glass Fibers [4, 8, 9].

Fiber	Compositions (wt%)												
	SiO_2	B_2O_3	Al_2O_3	CaO	MgO	ZnO	TiO_2	Zr_2O_3	Na_2O	K_2O	Li_2O	Fe_2O_3	F_2
General-purpose fibers													
Boron-containing E-glass	52-56	6-4	15-Dec	21-23	0.4-4		0.2-0.5		0-1	Treace		0.2-0.4	0.2-0.7
Boron-free E-glass	59		12.1	22.6	3.4		1.5		0.9	...		0.2	...
	60.1		13.2	22.1	3.1		0.5		0.6	0.2		0.2	0.1
Special-purpose fibers													

ECR-glass	58.2	...	11.6	21.7	2	2.9	2.5	...	1	0.2<1.3	..	0.1	Trace
D-glass	74.5	22	0.3	0.5	...			..	1	0.1	..	..	.
	55.7	26.5	13.7	2.8	1			..	0.1	..	0.1	..	
	60-65.5	...	23-25	0-9	6-11			0-1	0-0.1	..	..	0-0.1	
S-, R-, and Te Glass	99.999	...		...	...			..			..	..	
Silica/quartz													

Table 3: Physical and Mechanical attribution of the glass fibers [4, 8, 9].

	Coefficient of linear expansion	Specific heat	Dielectric constant at room temp.	Dielectric strength,	Volume resistivity at room temp.	Weight loss in 24h in 10%	Tensile strength at 23°C (73°F)	Young's modulus	Filament elongation at break, %		
Fiber	10-*°C	cal/g/°C	and 1 MHz	kV/em	log; 9(Q cm)	H,S0O,, %	MPa ksi	2Pa 10° psi			
Boron-containing	4.9-6.0	0.192	5.86-6.6	103	22.7-28.6	~41	3100-	450-551	76-78	11.0-11.3	4.5-1.9
E-glass	6		7	102	28.1	~6	3800	450-551	80-81	11.6-11.7	4.6
Boron-free							3100-				
E-glass							3800				
ECR-glass	5.9	a	a	500	1.576	3100-3800	450-551	80-81	11.6-11.7	4.5-4.9	
D-glass	3.1	0.175	3.56-3.62	130	1.47	2410	349	a	oa	aoe	
S-glass	2.9	0.176	4.53-4.6		1.523	4380-4590	635-666	88-91	12.8-13.2 |]	5.458	
Silica quartz	0.54		3.78		1.4585	3400	493	69	10	5	

E-Glass fiber

Commonly known as electrical-glass fiber (E-glass), this type of glass is classified as calcium alumino-borosilicate and typically contains less than 1% of alkali oxide, specifically Na2O. Many glass formulations incorporate a small quantity of fluoride, which aids in the raw material melting process and reduces the glass's liquidus temperature. E-glass, on occasion, exhibits a density of 2.62 g/cm3 and a refractive index of 1.562 [4].

Over extended periods of production, the composition of E-glass tends to fluctuate due to various factors that prompt manufacturers to reevaluate the formulation. The necessity to curtail environmental pollution resulting from emissions like gasses and dust from E-glass furnaces introduces production challenges and escalates raw material expenses. Similarly, the desire to enhance certain attributes such as corrosion resistance and the heightened mechanical capabilities of the final composite products drives the development of novel glass fiber variants (Tables 2, 3) [3, 4, 9].

Table 3 illustrates the progression in the development of commercial E-glass. Initially, the production of E-glass commenced with a boron-free glass composition. In 1943, the introduction of boron led to a reduction in processing temperature from 1288°C to 1200°C. Subsequently, in 1951, the cost of the batch was lowered by decreasing the B2O3 content from 10% to 5%–7%. Notably, the amount of MgO was also significantly decreased, establishing the standard formulation for E-glass. By the 1960s, the emission of boron and fluorine into the atmosphere from commercial furnace melts raised environmental and health concerns. In response, costly pollution control measures prompted the design of new E-glass compositions that were free from fluorine and essentially boron, and these entered the market in 1996 [4, 9].

AR Glass Fiber

In certain particular uses such as reinforcing cement and concrete, alkali-resistant (AR) glasses are employed, characterized by the inclusion of ZrO2. The presence of ZrO2 (ranging from 1% to 18%), combined with elevated levels of alkali oxides (Na2O+K2O, ranging from 11% to 21%) and TiO2 (ranging from 0% to 12%), contributes to the augmentation of alkali-resistant characteristics [10].

The Leibniz Institute of Polymer Research Dresden produces Alkali Resistance-Glass fibers (IPF ARG) utilizing a continuous pilot plant spinning equipment [11, 12]. The filament diameter was adjusted between 13, 17, and 19 micrometers by controlling the take-up speed of the spin cake winder. During the continuous spinning process, the filaments are treated with an alkali-resistant

sizing compound. This compound contains a silane coupling agent, specifically c-aminopropyltriethoxysilane (APS), and N-propyltrimethoxysilane (PTMO), along with film formers and nanoparticles, all incorporated within an aqueous sizing solution [11].

S-Glass Fiber

The patent for S-glass, assigned to Owens Corning under US Patent 3,402,055 [13], outlines its composition by weight: 55.0–79.9% SiO2, 12.6–32.0% Al2O3, and 4.0–20.0% MgO. Another variant, S-2 Glass, consists of 65% SiO2, 25% Al2O3, and 10% MgO, and is exemplified. Notably, S-glass is often used interchangeably with S-2 Glass, referring to glass compositions falling within the specifications outlined in ASTM Specification D 578. S-glass is part of a family of high-strength glasses [14]. Glasses within the S family exhibit a modulus approximately 20% higher than the more commonly used E-glasses. Although they don't reach the ultra high-modulus range exceeding 100 GPa, they strike a fine balance between high strength and high modulus. Conversely, ultra high-modulus glasses have been developed by incorporating additional oxides into base S-glass compositions. The combination of high strength, elevated elastic modulus, a high softening point, and a substantial elongation percentage (strain to failure) renders S-glass exceptionally well-suited for various applications, including ballistics, helicopter blades, pressure vessels, and aerospace composites [13].

R-Glass Fiber

R-glass is a type of fiber composition manufactured by Vetrotex, originating from the quaternary system of SiO2–Al2O3–CaO–MgO [13, 15]. When compared to S-glass, R-glass contains less SiO2 but an equivalent amount of Al2O3, with the remaining composition consisting of a combination of CaO and MgO. This unique combination enables the glass to maintain a relatively high softening temperature. However, the reduced SiO2 content and the resulting decrease in network connectivity also lead to a reduction in the tensile strength of the glass. At room temperature, the strength of R-glass is only about 85% of that exhibited by S-glass. Furthermore, while the modulus of R-glass matches that of S-glass, the elongation percentage or strain to failure is also approximately 85% of the value seen in S-glass. However, when subjected to elevated temperatures, the tensile strength of both R-glass and S-glass decreases to the point where they become equal, as illustrated in [13].

Properties and Characterizations

Mechanical Properties

Polymers serve as highly appealing matrix materials due to their ease of processing and relatively low density compared to other materials. They also demonstrate excellent mechanical properties. High-temperature resins are currently employed in the production of high-speed aircraft, rockets, and related space and electronic components as composite materials. In such composites, the primary load-bearing responsibility falls upon the reinforcements, particularly in cases where fiber reinforcements are dispersed within a less robust matrix (e.g., carbon/epoxy composites). Consequently, the overall strength and stiffness of these composites are predominantly determined by the strength and stiffness of the constituent fibers.

Tensile Properties

The glass fiber-reinforced polyester composite material was cut to the desired dimensions using a saw cutter. To prepare the composite for mechanical testing, the edges were finished using emery paper. Tensile testing was conducted using a universal testing machine (UH-F1000kN) with a crosshead speed of 5 mm/min in accordance with ASTM standards. Test specimens were prepared following ASTM D638 guidelines, measuring 165 x 19 mm with a thickness of 5 mm, as depicted in Figure 1. Three specimens underwent tensile testing, and their values were recorded [16].

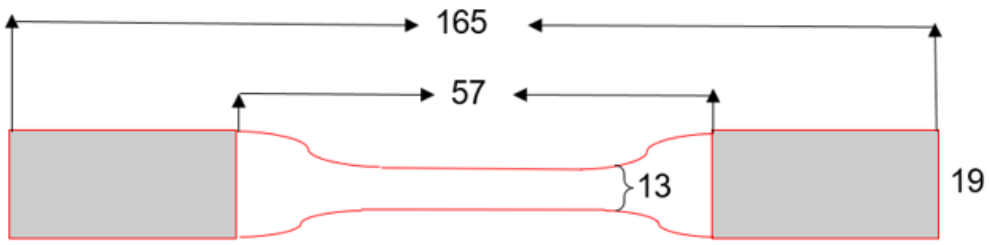

Figure 1: The geometries and dimensions of the specimen.

The properties of these composites are notably affected by the length of the fibers. The highest strength is attained when the fiber length within the laminate matches the critical fiber length. In the case of short fiber composites, strength depends on factors such as the fiber type, matrix, fiber length, fiber orientation, fiber concentration, and the bonding between the fiber and matrix. To prepare these composites, variations are made in both fiber length and fiber content. Subsequently, specimens for tensile, flexural, and shear testing are obtained from the composite plates in accordance with ASTM standards and are then tested using an Instron universal testing machine [17].

Table 4: The mechanical properties of short fiber composites at different fiber lengths [17].

Fiber Length (mm)	Fiber wt(%)	Tensile strength (MPa)	Tensile modulus (MPa)	Impact strength (J/cm2)
30	41	26.2	1398.3	1.75
	49	35.04	1168	6.59
	54	39.83	1405.62	7.12
40	32	26.05	1395.35	4.4
	36	28.96	1379.04	4.41
	42	31.04	1379.04	4.97
50	31	26.3	1315	6.24
	37	32.03	1312	6.38
	42	32.58	1106	7.62
	55	42.65	1515.2	6.05

The test results are presented in Table 4, indicating that composites consisting of 50 mm long fibers and 55 wt% fiber content exhibit the highest mechanical properties. Consequently, this study adopts 50 mm long fibers with a total fiber content of 55%. Rectangular specimens are extracted from the hybrid composite plate and subjected to testing on an Instron universal testing machine, with a crosshead speed of 1 mm/min. The ensuing results are discussed below, with four specimens tested for each weight ratio.

Bending Test

The flexural strength of the composite material specimens was investigated using a three-point bending test. This test was conducted utilizing a universal testing machine with a full-scale load capacity of 1000 kN and a crosshead speed of 5 mm/min, following the ASTM standard D-790. The specimens measured 80 mm x 12.5 mm in dimensions, with a thickness of 5 mm. The flexural strength of the composite material was calculated using equation (1) [16, 18].

$$\sigma\, force = \frac{3LF}{2t^2 w} \tag{1}$$

In the equation, F represents the applied load in Newtons (N), L is the support span in millimeters (mm), and w and t denote the width and thickness of the specimen in millimeters (mm), respectively.

Hardness test

The Brinell hardness test was conducted on the specimen employing a standard Brinell hardness tester. A load of 300 kgf (kilogram-force) was applied to the specimen for a duration of 30 seconds using a 5 mm diameter hard metal ball indenter. Subsequently, the indentation diameter was measured using a microscope equipped with an ocular, typically graduated in tenths of a millimeter, enabling estimations to the nearest 0.05 mm. It's important to note that the specimen surfaces were required to be smooth and free of oil and dirt for accurate results. Hardness measurements were taken at three distinct locations on the specimen, and the average value was calculated. The indentation was measured, and the hardness was calculated using equation (2) [16].

$$H = \frac{F}{\frac{\pi}{2} D\left(D - \sqrt{\left(D^2 - D_i^2\right)}\right)} \tag{2}$$

Here,

- H represents the hardness value.
- F is the applied load in kgf.
- D is the diameter of the ball indenter in mm.
- D_i is the diameter of the impression in mm.

To ensure accurate results, it is advisable to limit the test load in such a way that the impression diameter falls within the range of 2.5 to 4.75 mm.

Impact test

Toughness of the composite specimens was assessed using a Charpy impact tester (PIT Series) equipped with a U-shaped pendulum capable of delivering up to 150 J of energy. The impact energy of the composite material was determined following the ASTM D-256 standard. The impact energy was calculated by measuring the energy absorbed by the material just before it fractured, as described by equation (3) [16].

$$Impact\ strenght = \left(U_{abs} \div A\right) \tag{3}$$

The impact energy, denoted as U_{abs} (measured in Joules, J), was calculated by dividing the energy absorbed by the material during the test by the area of the cross-section of the specimen, represented as A and measured in square meters (m^2). Impact strength is typically expressed in Joules per square meter (J/m^2), and in this case, the notch depth is specified as 2 mm. For statistical reliability, each test was conducted using a total of five samples at room temperature (25 Degree Celsius) [16].

Molecular Characterizations

The total sizing on the fibers was determined through loss on ignition (LOI) analysis. The average fiber diameter was calculated

by considering the measured tex, the measured unsized fiber density, and the number of filaments/tow. The extraction of glass fibers was performed using a Soxhlet apparatus, with spectroscopic grade acetone (Fisher Scientific) as the solvent, for a duration of 2 hours. The fibers were weighed before and after extraction, and the solids content of the extracts was measured to ensure a proper material balance. The selection of acetone as the extraction solvent was based on its ability to model the solubility of resins of interest, determined through the estimation of solubility parameters using group contribution methods [19].

FTIR (Fourier-transform infrared) analysis was conducted using a Nicolet MAGNA-IR 860 spectrometer in transmission mode, equipped with a DTGS detector and KBr windows. A minimum of 100 scans were averaged for each analysis. The films were applied onto NaCl crystals and allowed to dry before analysis. The sample chamber underwent thorough purging before each analysis to ensure accuracy. Pure component samples were employed to identify significant peaks, and original sizing samples served as references for mixtures. At least two significant peaks were identified for each component to enable the separation of overlapping absorbances. Component concentrations were determined by measuring the absorbance relative to the concentration of the film former in both the sizing and the extract residue [20].

Molecular weight analysis was conducted utilizing High-Performance Liquid Chromatography (HPLC) with a Perkin Elmer 200 LC instrument and size exclusion chromatography (SEC) columns (Polymer Laboratories PLGel, Mixed-C, and 5 mm). HPLC-grade acetone from Aldrich was employed as the eluent. Molecular weights of the fractions were determined employing a multi-angle laser light scattering (MALLS) detector, specifically the Wyatt Technology miniDAWN, and concentration was measured using a differential refractive index (DRI) detector, the Wyatt Technology Optilab DSP."

X-ray Photoelectron Spectroscopy (XPS) analysis of the fiber samples was conducted using a Kratos AXIS 165 instrument equipped with an 8 detector hemispherical analyzer and a monochromatic Al Ka 1486.6 eV source. The instrument operated at 12 mA, 12 kV, and maintained a nominal vacuum level of 2 × 10^-9 Torr with a spot size of 0.5 cm^2. High-resolution scanning with a 40eV pass energy was employed to obtain all quantitative data. Tuning of the instrument was performed prior to the first analysis of each sample.

The C/O ratio on the surface of each fiber was determined by measuring the total surface carbon (C1s) at a 90° take-off angle and attributing the oxygen to the sizing. The oxygen signal, as indicated by the O1s peak, was separated into two components: one originating from the sizing and the other from the bare glass. The contribution of the O1s signal solely from the glass was estimated using the XPS-measured ratio of O/Ca for bare glass fibers, in conjunction with the measured Ca concentration in each sample. So the equation

$$o_{sizing} = o_{measure} \times Ca_{measure} \times \frac{o}{Ca} of\left(base\ glass\right)$$

Bare glass fibers, referred to as water-sized fibers, are fibers produced during the same production campaign as the sized fibers. These bare fibers were subjected to argon sputtering before XPS analysis. In samples with excellent sizing coverage and a high C/Ca ratio, the contribution from the glass to the O1s signal was minimal. The C/O ratio of the sizing was calculated based on the concentrations of known components in the sizing material. Calcium (Ca) was selected as the reference element for the glass, as it is absent in the sizings but present in the glass. On the other hand, silicon (Si) can be found in both the sizing and the glass due to the presence of silane [19, 20].

Thermo-gravimetric Analysis (TGA)

Thermo-gravimetric analysis (TGA) was conducted using a TA Q500 instrument. The tests were performed within a temperature range of 0 to 800 degrees Celsius under an air atmosphere. Specimens with varying clay content, including pure polyester (0% clay), 0.5% clay, 1% clay, 1.5% clay, and 2% clay, were subjected to thermo-gravimetric analysis.

Table 5: Impact test results [21].

% wt. of filler	Thickness of the specimen in mm	Specimen width in mm	Impact energy (specimen) in J	impact energy in J/m	Impact strength kJ/m2	aColor in Graph Picture (1)
0	0.479	12.86	0.76	1089.4	84.71	Dark Blue
0.5	0.875	12.81	1.05	1054.94	84.03	Red
1	0.936	12.93	0.59	1191.94	92.69	Green
1.5	0.941	12.77	0.92	988.62	76.88	Blue
2	1.203	12.84	0.97	1024.8	80.09	Cyan

Thermal Analysis from Table (5)

Figure (2) illustrates the variation in percentage weight loss and percentage differential weight as the temperature increases from room temperature to 800°C for five different samples, namely those with 0%, 0.5%, 1%, 1.5%, and 2% weight of nanoclay blended into nanocomposite materials. In the nanocomposite, the curing rate was observed to increase with the addition of clay compared to the pure polyester FRP. For all blends, the weight loss remained constant up to 150°C, after which decomposition began, occurring roughly between 150°C and 200°C. The curve does not show a sig-

nificant shift in the degradation temperature with varying clay content, although minor variations may be attributed to fluctuations in moisture content. The degradation continues with a consistent pattern up to 320°C, resulting in a weight loss of approximately 10%. The second phase of degradation initiates around 320°C, with a steady weight loss observed across different clay-filled samples, approximately 25%. This suggests that the decomposition temperature of the nanocomposite has shifted to higher temperatures, indicating improved thermal stability of the polymer with up to 2% clay content. The presence of inorganic materials within the polymer matrix typically enhances the thermal stability of nanocomposites. The weight-loss temperature curve indicates that the residue remaining beyond 400°C aligns with the inorganic material content of each sample. [21, 22]. The degradation process commenced at around 150–200 degrees Celsius and concluded at approximately 300 degrees Celsius, resulting in a mass loss percentage of 10%. These losses are attributed to the thermal degradation of the alkyl tails (-CH2) and ammonium heads (-N (CH3)3) [23].

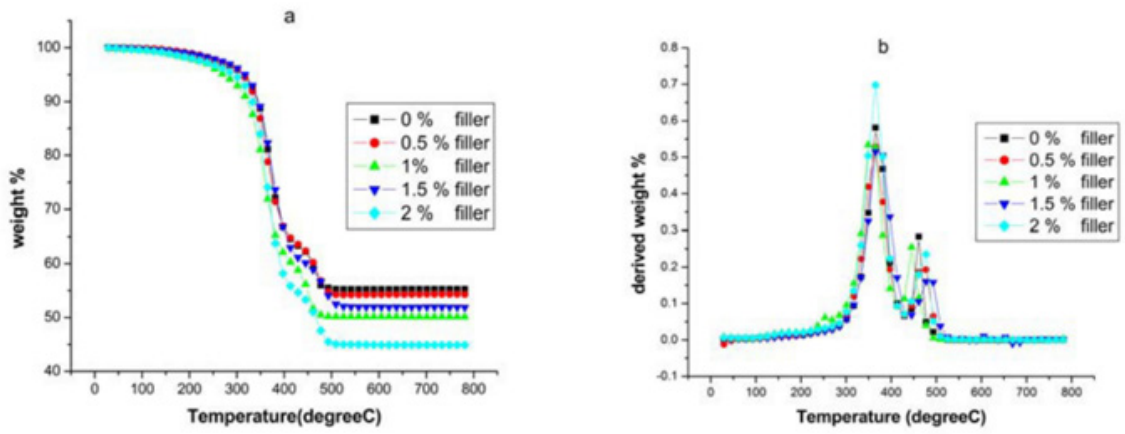

Figure 2: Thermo-gravimetric analysis, variation of (a) % weight and (b) % derived weight with temperature [21].

Electronic and Electrical Properties

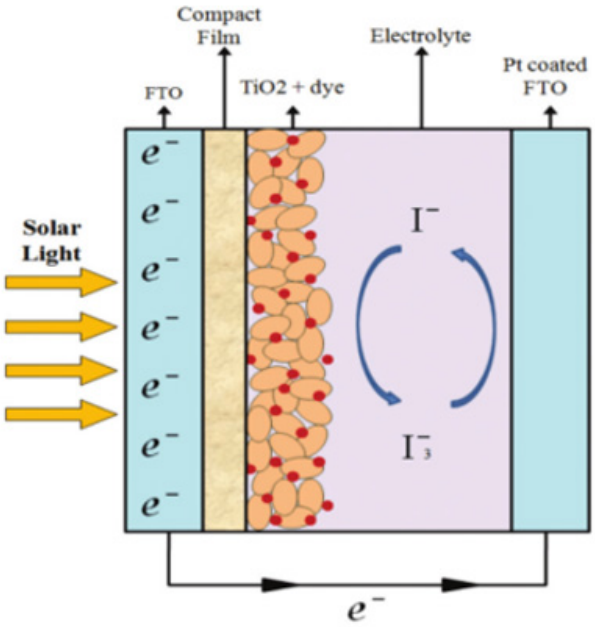

Figure 3:

To evaluate the uniformity of coating and its impact on electronic properties, we subjected glass fibers to different oxygen plasma treatment conditions. The introduction of an oxygen-rich hydrophilic layer onto the glass fibers facilitated optimal adhesion of Ti3C2Tx MXene, resulting in the best coating. Figure 4a and 4b display scanning electron microscope (SEM) images of fractured surfaces of plasma-treated fibers at varying plasma power intensities (50 and 150 W) after being dipped five times in an aqueous MXene dispersion containing large flakes. In both cases, MXene coverage is apparent, with visible Ti3C2Tx flakes adhering to the fiber surfaces. However, at higher intensity (150 W), a thicker but less uniform MXene coating is obtained. The coating at 150 W has more MXene adhering to the glass fiber surface, but it is less uniform and contains visible aggregates of large Ti3C2Tx flakes. Corresponding plots of electrical resistance for different plasma power levels and treatment durations are presented in Figure 4c and 4d. Fiber bundles treated at 150 W power with a maximum of 50 dips exhibited the lowest resistance properties, measuring approximately 2.5 ± 0.47 kΩ. In contrast, those treated at 50 W showed slightly higher resistance values, averaging 14 ± 9.6 kΩ (Figures 4c and 4d). At higher plasma power, the induced hydrophilic surface of the treated glass fibers facilitated improved interaction with oxygen-containing functional groups on the MXene surface [24, 25]. When analyzing dip-coated fibers treated at 50 W, we noticed a slight rise in electrical resistance after five dips (for 20 and 50 dips); nevertheless, the overall resistance did not exceed 110 kΩ. At lower plasma power levels, it is likely that there are fewer oxygen groups covering the surface of the glass fibers compared to the 150 W treatment. This results in fewer MXene flakes adhering to the glass surface and participating in electronic pathways. Regarding the treatment duration for both 50 and 150 W, only minor changes in electrical resistance were observed when increasing from 0.5 to 5 minutes of plasma exposure (25 kΩ or less). Fibers treated at 150 W consistently exhibited lower electrical resistances due to the hydrophilic nature of the glass fibers, which allows for maximum MXene coverage. In cases where the MXene coating on fibers lacks uniformity, it can lead to poor damage-monitoring capabilities because the coating may easily be removed during testing. Consequently, we used glass fibers treated at 50 W for 5 minutes to assess the damage-monitoring capabilities of MXene-coated fibers [24, 25].

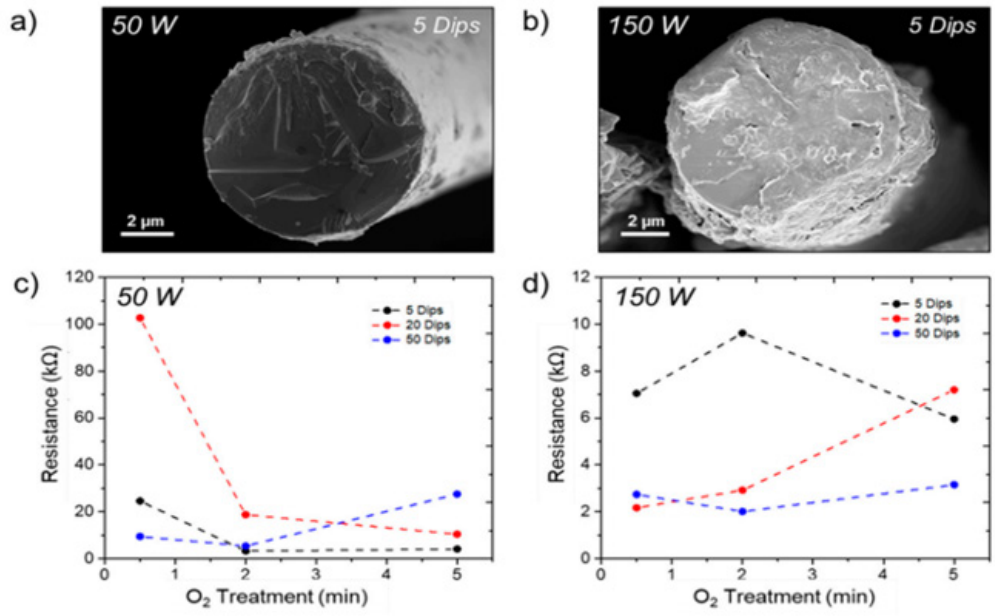

Figure 4: This figure illustrates a comparison of MXene coatings based on oxygen plasma surface treatment and their corresponding resistance values. In the SEM images (a) and (b), you can observe Ti3C2Tx-coated fibers treated with plasma at 50 W and 150 W power, respectively. The resistance values for different surface treatment times are shown in (c) and (d). The lines connecting the data points in (c) and (d) are intended to assist in visualizing trends. These resistance values provide insight into the electrical properties of the MXene-coated fibers under various treatment conditions, with different plasma powers and treatment times [24].

Table 6: In the context of high-voltage insulator core rod applications, the electrical properties of glass fiber-reinforced epoxy composites are of paramount importance [26].

Composites	Processing Method	Electrical Resistivity (Ω.m)	Dielectric strength (MV/m	Reference
Epoxy/low surface density fiberglass	Manually	1.614×109		27
E-glass/epoxy	Pultrusion		Improved	28
Low-seed ECRglass/epoxy	Pultrusion	Improved		26
ECR-glass/epoxy	Pultrusion		Improved	29
80 vol. %/epoxy	Laser sintering		Improved	30

Glass fiber/epoxy		Improved		31, 32
10 wt AIN/50 wt%/ glass fiber/epoxy	Hand lay-up	Improved	Improved	33
E-glass/epoxy	Filament winding/ Burn-of		Improved	34
E-glass/epoxy	Hand lay-up	Improved		35
Glass fiber/epoxy	Pultrusion			36
E-glass fiber/epoxy	Pultrusion	Decreased	Decreased	37

E-Glass/Vinyl Ester Epoxy Composite (Graph a):

The x-axis represents the moisture content, typically measured in percentage or parts per million (ppm). The y-axis represents the leakage current, typically measured in microamperes (μA) or some other current unit. As moisture content increases along the x-axis, the leakage current is observed on the y-axis. The graph should exhibit a linear trend, which indicates a proportional relationship between moisture content and leakage current. This means that as moisture content increases, the leakage current also increases in a consistent manner. The slope of the linear trend line (indicated as "ft" in your description) represents the rate at which the leakage current increases with moisture content. A steeper slope suggests a more significant impact of moisture on electrical behavior.

E-Glass/Polyester Composite (Graph b):

Similar to graph a, the x-axis represents moisture content, and the y-axis represents leakage current. For the E-glass/polyester composite, the graph may show a similar linear trend as in graph a, with moisture content affecting the leakage current. However, the slope of the linear trend line and the overall behavior of the graph may differ from that of the vinyl ester epoxy composite, as different composite materials can respond differently to moisture.

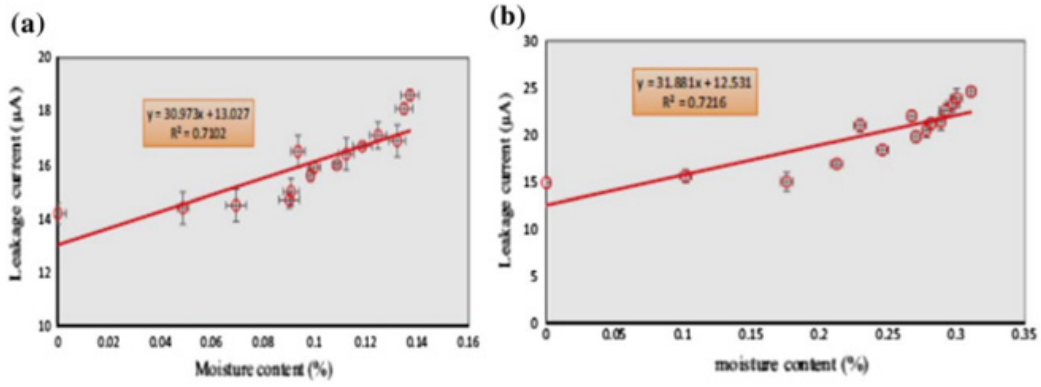

Figure 5: The "leakage current versus moisture content" graph is a crucial representation of how the electrical behavior of composite materials changes with varying levels of moisture content. Here's a description of the graph for both E-glass/vinyl ester epoxy and E-glass/polyester composites [26, 37].

These graphs are essential for understanding how moisture affects the electrical properties of composite materials, which is crucial for applications where maintaining electrical insulation and preventing leakage currents are critical, such as in electrical insulators or high-voltage equipment. The linear trend lines provide valuable information about the material's moisture sensitivity and can help in designing materials for specific environmental conditions.

General Application of Glass Fiber

Aircraft and Military Applications

The early applications of fiber-reinforced polymers (FRPs) in commercial aircraft marked a significant shift in aircraft design and manufacturing [7]:

Table 7

Aircraft	Component	Material	Overall Weight Saving Over Metal Component (%)
F-14 (1969)	Skin on the horizontal stabilizer box	Boron fiber–epoxy	19
F-11	Under the wing fairings	Carbon fiber–epoxy	
F-15 (1975)	Fin, rudder, and stabilizer skins	Boron fiber–epoxy	25
F-16 (1977)	Skins on vertical fin box, fin leading edge	Carbon fiber–epoxy	23

F=A-18 (1978)	Wing skins, horizontal and vertical tail boxes; wing and tail control surfaces, etc.	Carbon fiber–epoxy	35
AV-8B (1982)	Wing skins and substructures; forward fuselage; horizontal stabilizer; flaps; ailerons	Carbon fiber–epoxy	25

Space Applications

The foremost rationale behind the utilization of fiber-reinforced composites in numerous spacecraft is to achieve substantial weight reduction [7, 5]. These materials find diverse applications in the construction of space shuttles, including: The mid-fuselage truss structure, which employs aluminum tubes reinforced with boron fibers. The payload bay door, consisting of a sandwich structure featuring carbon fiber-reinforced epoxy face sheets and an aluminum honeycomb core. The remote manipulator arm, crafted from an ultrahigh-modulus carbon fiber-reinforced epoxy tube. Pressure vessels, reinforced with Kevlar 49 fiber-reinforced epoxy. In all of these cases, the primary objective is to reduce weight while maintaining structural integrity in space vehicle components.

Moreover, fiber-reinforced polymers play a pivotal role in providing support structures for various smaller components, including solar arrays, antennas, optical platforms, and the like, in addition to their application in substantial structural elements. A crucial factor in their selection for these purposes is their ability to maintain dimensional stability across a broad temperature range. Many carbon fiber-reinforced epoxy laminates can be engineered to achieve a coefficient of thermal expansion (CTE) close to zero. Comparable CTE values are found in certain aerospace alloys like Invar. However, carbon fiber composites offer the advantages of lower density, greater strength, and a higher stiffness-to-weight ratio. This unique combination of mechanical properties and CTE has led to various applications for carbon fiber-reinforced epoxies in artificial satellites. One notable application is in the support structures for mirrors and lenses within space telescopes. Given the extreme temperature fluctuations in space, ranging from -100°C to 100°C, maintaining dimensional stability in the support structure is of paramount importance. Otherwise, significant shifts in the positions of mirrors or lenses due to thermal expansion or distortion could adversely affect the telescope's focusing capabilities [7].

Carbon fiber-reinforced epoxy tubes find applications in constructing truss structures for satellites in low Earth orbit (LEO) and interplanetary missions. These truss structures provide support for optical benches, solar panels, antenna reflectors, and various modules. Carbon fiber-reinforced epoxies are favored over metals or metal matrix composites due to their lower weight and exceptionally low coefficient of thermal expansion (CTE). However, one significant challenge faced by epoxy-based composites in LEO satellites is their vulnerability to degradation caused by atomic oxygen (AO) absorption from Earth's thin atmosphere at those altitudes. To counter this issue, protective measures are employed, such as wrapping the tubes with thin aluminum foils to shield them from AO exposure. There are additional concerns when using fiber-reinforced polymers in the space environment. These include outgassing of the polymer matrix when exposed to the vacuum of space and embrittlement resulting from particle radiation. Outgassing can lead to dimensional changes, while embrittlement may induce the formation of microcracks. If the outgassed substances deposit onto satellite components like sensors or solar cells, it could significantly impair their functionality [8].

Automotive Applications

Fiber-reinforced composites play a crucial role in the automotive industry, with applications falling into three main categories: body components, chassis components, and engine components.

Body Components: These include exterior body parts like hoods or door panels, which require high stiffness, damage tolerance (dent resistance), and a top-quality surface finish for appearance (often referred to as 'Class A' surface finish). These components are typically made from E-glass fiber-reinforced sheet molding compound (SMC) composites. In these composites, short glass fibers (usually around 25 mm in length) are randomly dispersed within a polyester or vinyl ester resin matrix. E-glass fiber is preferred over carbon fiber due to its considerably lower cost. The manufacturing process for SMC parts is compression molding. Achieving a 'Class A' surface finish with compression-molded SMC can be challenging, often requiring in-mold coating of the exterior surface with a flexible resin. However, for underbody and under-the-hood components where external appearance is less critical, SMC is commonly used. Examples of such components include radiator supports, bumper beams, roof frames, door frames, engine valve covers, timing chain covers, oil pans, and more [7]. This categorization reflects the diverse applications of fiber-reinforced composites in the automotive sector, where these materials are used to optimize various properties depending on the component's specific requirements.

Sporting Goods Applications

These items represent a wide range of sporting and recreational equipment that commonly use fiber-reinforced composites to enhance their performance and durability:

1. Tennis Rackets: Fiber-reinforced composites are used in the construction of tennis racket frames to provide strength and stiffness while maintaining a lightweight design.
2. Racquetball Rackets: Similar to tennis rackets, racquetball rackets benefit from the use of fiber-reinforced materials for improved performance.
3. Fishing Rods: Fishing rods utilize composite materials to achieve a balance of sensitivity, flexibility, and strength.
4. Bicycle Frames: High-performance bicycles often feature frames made from carbon fiber composites, which provide excellent strength-to-weight ratios.
5. Snow and Water Skis: Skis, both for snow and water, use composites to achieve the necessary stiffness and responsiveness.
6. Ski Poles and Pole Vault Poles: These poles require lightweight and durable materials, making composites an ideal choice.

7. Hockey Sticks: Hockey sticks are designed to be lightweight yet sturdy, making composites a popular choice for construction.
8. Baseball Bats: Baseball bats benefit from the use of composite materials for improved performance, including enhanced energy transfer.
9. Sailboats and Kayaks: The hulls and components of sailboats and kayaks often use composites for their lightweight and durable properties.
10. Oars and Paddles: The use of composites in oars and paddles helps to reduce weight while maintaining strength.
11. Canoe Hulls: Canoes may incorporate composite materials to enhance their durability and performance.
12. Surfboards and Snowboards: Both surfboards and snowboards use composites to provide the ideal combination of flexibility and strength.
13. Arrows: Arrows used in archery may incorporate composite materials to enhance accuracy and durability.
14. Archery Bows: Modern archery bows often feature composite materials to optimize their performance.
15. Javelins: Javelins used in track and field may utilize composite materials for their lightweight yet aerodynamic design.
16. Helmets: Sports helmets, such as those used in cycling and skiing, may incorporate composites to provide impact resistance.
17. Exercise Equipment: Some exercise equipment, including weightlifting bars and frames, may benefit from the use of composites for durability and safety.
18. Athletic Shoe Soles and Heels: Composite materials can be used in the soles and heels of athletic shoes to provide cushioning and support.
19. Golf Club Shafts: Golf club shafts often incorporate carbon fiber composites to optimize the balance of flexibility and strength.

These applications demonstrate the versatility and advantages of fiber-reinforced composites in the world of sports and recreation, where they help enhance performance, durability, and overall user experience.

Marine Applications

Glass fiber-reinforced polyesters have been utilized in various boat types, including sailboats, fishing boats, dinghies, lifeboats, and yachts, since they were first introduced as a commercial material in the 1940s [38]. Today, nearly 90% of recreational boats are constructed using either glass fiber-reinforced polyester or glass fiber-reinforced vinyl ester resin. These materials are used in various boat components such as hulls, decks, and interior parts. The manufacturing process commonly employed for producing these components is contact molding. Despite being labor-intensive, this process is cost-effective due to its low equipment expenses, making it accessible to many small boat-building companies. In recent years, Kevlar 49 fiber has started replacing glass fibers in certain applications within the boating industry. This shift is driven by Kevlar's higher tensile strength-to-weight and modulus-to-weight ratios compared to glass fibers. Kevlar finds use in boat hulls, decks, bulkheads, frames, masts, and spars, primarily offering the advantage of weight reduction, resulting in improved cruising speed, acceleration, maneuverability, and fuel efficiency.

Carbon fiber-reinforced epoxy is a material of choice in the construction of racing boats, where achieving weight reduction is of utmost importance to gain a competitive edge. These boats utilize carbon fiber-reinforced epoxy laminates extensively, encompassing the complete hull, deck, mast, keel, boom, and various other structural components. Additionally, sandwich laminates are employed, featuring carbon fiber-reinforced epoxy skins in combination with either honeycomb or plastic foam cores. To enhance impact resistance and further reduce the boat's weight, carbon fibers are sometimes combined with other fibers possessing lower density and higher strain-to-failure characteristics, such as high-modulus polyethylene fibers. This strategic use of materials contributes to improved performance and competitiveness in racing.

The use of composite materials in naval ships dates back to the 1950s and has seen continuous growth ever since [39]. These materials are applied in various components of ships, including hulls, decks, bulkheads, masts, propulsion shafts, rudders, and more, spanning mine hunters, frigates, destroyers, and even aircraft carriers. A prominent example of the extensive use of fiber-reinforced polymers can be observed in the Royal Swedish Navy's Visby-class corvette, a colossal 72 meters in length and 10.4 meters in width, marking it as the largest composite ship globally. Furthermore, the US Navy has recently commissioned the construction of a 24-meter-long combat ship named Stiletto, with its primary construction material being carbon fiber-reinforced epoxy. This choice is rooted in the ship's design prerequisites, which demand lightweight and high-strength properties for achieving high speed, maneuverability, extended range, and substantial payload capacity. Additionally, the stealth characteristics of these ships play a crucial role in minimizing radar reflection.

Radiation Effect

The mechanical properties, including tensile strength (TS), bending strength (BS), tensile modulus (TM), bending modulus (BM), impact strength (IS), and hardness, of three different materials were evaluated: the matrix PP, silk fiber/PP composite, and E-glass fiber/PP composite. The results indicated that the incorporation of fibers significantly improved the mechanical properties of both composites. Specifically, TS, BS, TM, BM, and IS all showed significant increases due to the fiber reinforcement [40].

However, there was a notable reduction in the percentage of elongation at break (Eb%) in the composites compared to pure PP. This reduction can be attributed to the inherently low Eb% of the fibers in comparison to PP.

For reference, the mechanical properties of the pure PP sheet were as follows:

- Tensile Strength (TS): 21 MPa

- Tensile Modulus (TM): 535 MPa
- Elongation at Break (Eb%): 318%
- Bending Strength (BS): 29 MPa
- Bending Modulus (BM): 1950 MPa
- Impact Strength (IS): 4.3 kJ/m2
- Hardness: 95 Shore A

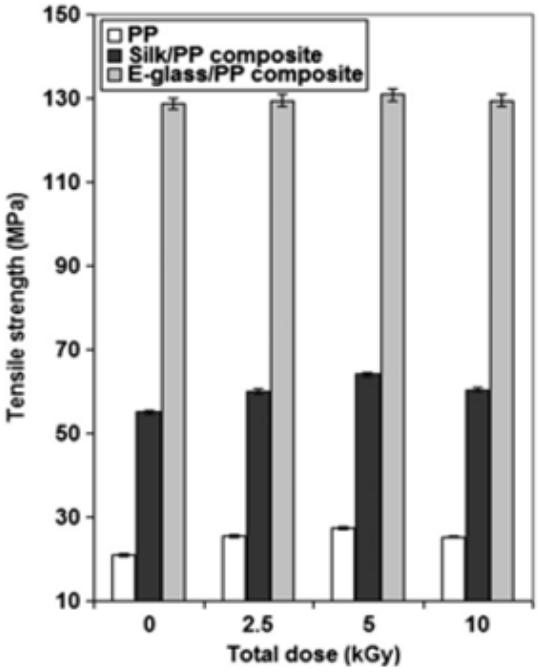

Figure 5(a): Effect of gamma radiation on tensile strength of polypropylene sheet and the composites.

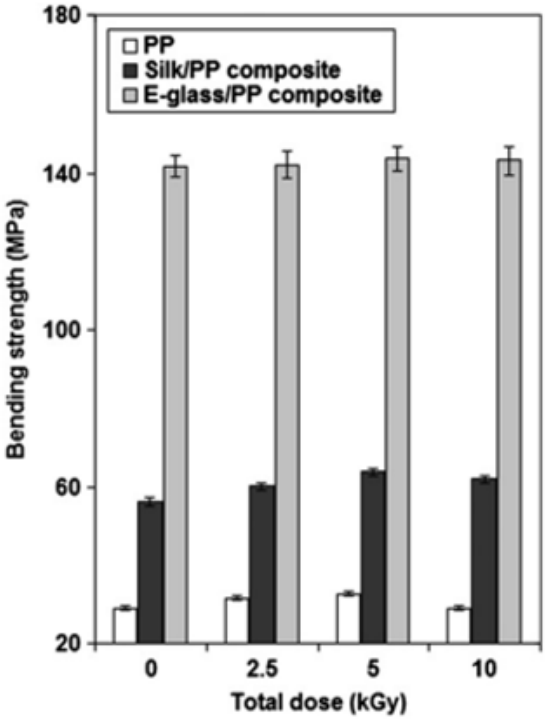

Figure 5 (b): Effect of gamma radiation on bending strength of polypropylene sheet and the composites.

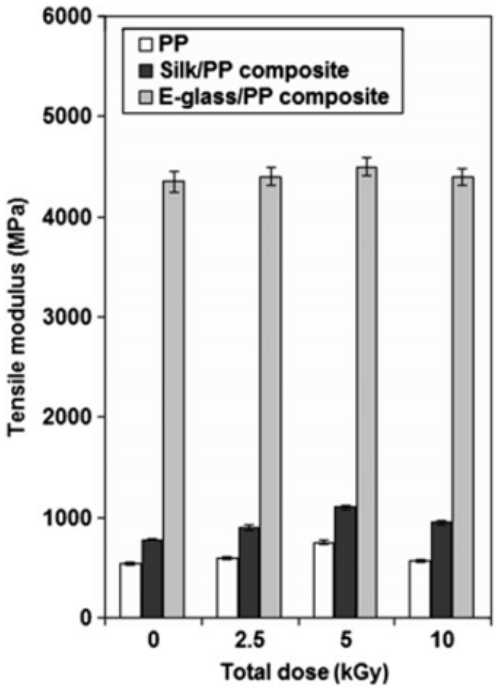

Figure 5(c): Effect of gamma radiation on tensile modulus of polypropylene sheet and the composites.

Benefits and Drawbacks

Electrical-Glass Fiber

Table (8): Benefits and drawbacks of E-Glass Fiber [6, 8].

Benefits	Drawbacks
Affordability and rapid production rates.	
Comparatively light weight	Denser in comparison to carbon and organic fibers.
	Modest tensile modulus
Capable of retaining strength properties across a broad spectrum of conditions.	Without treatment, it exhibits self-abrasiveness, and abrasion can lead to a decrease in tensile modulus.
Exhibits limited sensitivity to moisture.	Shows relatively modest fatigue resistance.
Resistant to chemicals.	Chloride ions corrode and dissolve the surface of E-glass.
Not flammable and exhibits heat resistance.	

Electrical glass fiber has some benefits and drawbacks. It will depend on its uses where it should be used. In the bellow table showing a comparison.

Conclusion

This comprehensive review delves into the mechanical, dynamic, tribological, thermal, and water absorption properties of GFRP (Glass Fiber Reinforced Polymer) composites. It underscores the significant applications of these composites in various fields. Specifically, when it comes to selecting materials for high-voltage insulator core rods, glass fiber-reinforced epoxy composites, including E-glass and ECR-glass, have consistently emerged as preferred choices. However, the review highlights certain challenges that glass fiber-reinforced epoxy composites face in composite insulator applications. These challenges encompass issues such as brittle fracture due to stress corrosion cracking and fracture caused by abnormal heating. Such problems can lead to a decline in the mechanical and electrical insulation properties during operation. Consequently, there is a pressing need for further advancements in glass fiber-reinforced epoxy composites to ensure their effectiveness in load-bearing support and electrical insulation within high-voltage transmission networks. The review offers insights into past research efforts aimed at enhancing the properties of glass fiber-reinforced epoxy composites for use as core rods in high-voltage composite (non-ceramic) insulator applications. Additionally, it outlines potential avenues for future research. One promising direction is

the modification of the epoxy matrix by incorporating polyimide to develop glass fiber-reinforced epoxy composite insulator core rods. Another avenue involves the incorporation of insulator nanomaterials into glass fiber-reinforced epoxy matrix composites, with a focus on optimizing the manufacturing process. These approaches hold significant potential for advancing glass fiber-reinforced epoxy composites for insulator core rod applications.

Acknowledgment

The research work was supported by the Annual Development Project (ADP) of Bangladesh Government. The title of the project is: "Strengthening of existing gamma source of Bangladesh Atomic Energy Commission". Special thanks to The Ministry of Science and Technology and The Ministry of Planning, Government of the People's Republic of Bangladesh.

Conflicts of Interest

All authors state that there is no conflict of interest.

References

1. AT DiBenedetto (2001) Tailoring of interfaces in glass fiber reinforced polymer composites: a review. Materials Science and Engineering: A 302(1): 74-82.
2. TP Sathishkumar, S Satheeshkumar, J Naveen (2004) Glass fiber-reinforced polymer composites-a review 33(13): 1258-1275.
3. Lowenstein KL (1983) The manufacturing technology of continuous glass fibers. Amsterdam: Elsevier pp. 209-227.
4. Cevahir A (2017) Glass fibers in fiber technology for fiber-reinforced composites. Woodhead Publishing pp. 99-121.
5. M Zhang, J P Matinlinna (2011) E-Glass Fiber Reinforced Composites in Dental Applications. Silicon 4(1): 73-78.
6. J Wiley (1988) The Fiberglass Repair and Construction Handbook. McGraw Hill Professional pp. 156-312.
7. Mallick, Pankar K (2007) Fiber-reinforced composites: materials, manufacturing, and design. CRC press pp. 312-256.
8. D B Miracle, S L Donaldson (2001) Introduction to Composites. dl.asm international.org 21: 3-17.
9. F T Wallenberger, P A Bingham, Springerlink (2010) (Online Service, Fiberglass and Glass Technology): Energy-Friendly Compositions and Applications. New York, Ny: Springer Us pp. 121-365.
10. Velez, Mariano (2019) Proceedings: 15th Asia-Pacific Federation for Clinical Biochemistry and Laboratory Medicine (APFCB) Congress. Indian Journal of Clinical Biochemistry 34(S1): 1-233.
11. C Scheffler, SL Gao, R Plonka, E Mäder, S Hempel, et al. (2009) Interphase modification of alkali-resistant glass fibers and carbon fibers for textile reinforced concrete I: Fibre properties and durability. Composites Science and Technology 69(3-4): 531-538.
12. Green, David J (1984) Compressive Surface Strengthening of Brittle Materials. Journal of Materials Science 19(7): 2165-2171.
13. Wallenberger, Frederick T (2010) Fiberglass and Glass Technology: Energy-Friendly Compositions and Applications. New York, Ny, Springer Us.
14. Thomas J A G (1971) USA Specifications for Composites: (1) ASTM Standards for Glass Fibre Reinforcement. Composites 2(2): 114-116.
15. R L Hausrath, A V Longobardo (2009) High-Strength Glass Fibers and Markets. Fiberglass and Glass Technology pp. 197-225.
16. M El-Wazery, M El-Elamy, S Zoalfakar (2017) Mechanical Properties of Glass Fiber Reinforced Polyester Composites. International Journal of Applied Science and Engineering 14: 121-147.
17. R Velmurugan, V Manikandan (2007) Mechanical properties of palmyra/glass fiber hybrid composites. Composites Part A: Applied Science and Manufacturing 38(10): 2216-2226.
18. M Davallo, H Pasdar (2009) Comparison of Mechanical Properties of Glass-Polyester Composites Formed by Resin Transfer Moulding and Hand Lay-Up Technique.
19. R L Gorowara, W E Kosik, S H McKnight, R L McCullough (2001) Molecular characterization of glass fiber surface coatings for thermosetting polymer matrix/glass fiber composites. Composites Part A: Applied Science and Manufacturing 32(3-4): 323-329.
20. E K Drown, H Al Moussawi, L T Drzal (1991) Glass fiber 'sizings' and their role in fiber-matrix adhesion. Journal of Adhesion Science and Technology 5(10): 865-881.
21. PP Binu, K E George, M N Vinodkumar (2016) Effect of Nanoclay, Cloisite15A on the Mechanical Properties and Thermal Behavior of Glass Fiber Reinforced Polyester. Procedia Technology 25: 846-853.
22. S Yang, J Taha-Tijerina, Verónica Serrato-Diaz, K Hernandez, K Lozano, et al. (2007) Dynamic mechanical and thermal analysis of aligned vapor grown carbon nanofiber reinforced polyethylene. Composites Part B: Engineering 38(2): 228-235.
23. J M Cervantes-Uc, J V Cauich-Rodríguez, H Vázquez-Torres, Luis Francisco Garfias-Mesias, D R Paul, et al. (2007) Thermal degradation of commercially available organoclays studied by TGA–FTIR. Thermochimica Acta 457(1-2): 92-102.
24. C B Hatter, A Sarycheva, A Levitt, B Anasori, L Nataraj, et al. (2020) Electrically Conductive MXene-Coated Glass Fibers for Damage Monitoring in Fiber-Reinforced Composites. C 6(4): 64.
25. L Verger, C Xu, V Natu, H M Cheng, W Ren, et al. (2019) Overview of the synthesis of MXenes and other ultrathin 2D transition metal carbides and nitrides. Current Opinion in Solid State and Materials Science 23(3): 149-163.
26. V E Ogbonna, A P I Popoola, O M Popoola, S O Adeosun (2021) A review on corrosion, mechanical, and electrical properties of glass fiber-reinforced epoxy composites for high-voltage insulator core rod applications: challenges and recommendations. Polymer Bulletin 79(9): 6857-6884.
27. Jaffer HI, Harair R, Ammar N, Mahdi Y, Noaman R, et al. (2015) Study the electrical insulation of polymeric composite. Al-Nahrain Journal of Science 18(2): 50-5.
28. Mohammad Reza Amini, Alireza Khavandi (2018) Evaluation of the electrical properties and mechanical behavior of insulator's composite core in harsh environments. Materials research express 5(11): 115306-115306.
29. K Wieczorek, P Ranachowski, Z Ranachowski, P Papliński (2020) Ageing Tests of Samples of Glass-Epoxy Core Rods in Composite Insulators Subjected to High Direct Current (DC) Voltage in a Thermal Chamber. Energies 13(24): 6724-6724.
30. Zhaoqing Li, Wangbing Zhou, Lei Yang, Peng Chen, Chunze Yan, et al. (2019) Glass Fiber-Reinforced Phenol Formaldehyde Resin-Based Electrical Insulating Composites Fabricated by Selective Laser Sintering. Polymers 11(1): 135.
31. B Wang, J Lu, Z Fang, Z Jiang, J Hu, et al. (2019) Development of antithunder composite insulator for distribution line. Ieej Transactions on Electrical and Electronic Engineering 15(1): 100-107.
32. Zhang L, Sun Q, Wang HC, Zhao XL, Hu JM, et al. (2019) Experimental study on the mechanical properties of E-glass fiber/epoxy composite material. Electric Power Construction/ Dianli Jianshe 31(9): 118-21.
33. P Panda, G Mishra, S Mantry, S K Singh, S P Sinha (2013) A study on mechanical, thermal, and electrical properties of glass fiber-reinforced epoxy hybrid composites filled with plasma-synthesized AlN. Journal of Composite Materials 48(25): 3073-3082.
34. B Kechaou, M Salvia, K Benzarti, C Turki, Z Fakhfakh, et al. (2011) Role of fiber/matrix interphases on dielectric, friction, and mechanical properties of glass fiber-reinforced epoxy composites. Journal of Composite Materials 46(2): 131-144.

35. Ogaili AA, Al-Ameen ES, Kadhim MS, Mustafa MN (2020) Evaluation of mechanical and electrical properties of GFRP composite strengthened with hybrid nanomaterial fillers. AIMS Materials Science 7(1): 93-102.

36. Nagaraj HP, Ravi KN, Vasudev N (2018) Brittle fracture of GRP rod used in polymeric insulators an experimental study. Int J Electr Electr Eng 7(2): 9-16.

37. Mohammad Reza Amini, Alireza Khavandi (2019) Synergistic effects of mechanical and environmental loading in stress corrosion cracking of glass/polymer composites. Journal of Composite Materials 53(24): 3433-3444.

38. D W Chalmers (1994) The Potential for the use of composite materials in marine structures. Marine Structures 7(2-5): 441-456.

39. A P Mouritz, E Gellert, P Burchill, K Challis (2001) Review of advanced composite structures for naval ships and submarines. Composite Structures 53(1): 21-42.

40. Q T H Shubhra, A K M M Alam (2011) Effect of gamma radiation on the mechanical properties of natural silk fiber and synthetic E-glass fiber reinforced polypropylene composites: A comparative study. Radiation Physics and Chemistry 80(11): 1228-1232.